ABRUPT CHANGES OF THE PHOTOSPHERIC MAGNETIC FIELD IN ACTIVE REGIONS AND THE IMPULSIVE PHASE OF SOLAR FLARES (Postprint)

E. W. Cliver, et al.

23 August 2012

Technical Paper

AIR FORCE RESEARCH LABORATORY
Space Vehicles Directorate
3550 Aberdeen Ave SE
AIR FORCE MATERIEL COMMAND
KIRTLAND AIR FORCE BASE, NM 87117-5776

NOTICE AND SIGNATURE PAGE

AFRL-RV-PS-TP-2014-0002 HAS BEEN REVIEWED AND IS APPROVED FOR PUBLICATION IN ACCORDANCE WITH ASSIGNED DISTRIBUTION STATEMENT.

//SIGNED//   //SIGNED//

Dr. Edward W. Cliver   Edward J. Masterson, Colonel, USAF
Program Manager, AFRL/RVBXS   Chief, Battlespace Environment Division

REPORT DOCUMENTATION PAGE

1. REPORT DATE *(DD-MM-YYYY)*	2. REPORT TYPE	3. DATES COVERED *(From - To)*
23-08-2012	Technical Paper	01 Oct 2010 to 30 Jul 2012

4. TITLE AND SUBTITLE	5a. CONTRACT NUMBER
Abrupt Changes of the Photospheric Magnetic Field in Active Regions and the Impulsive Phase of Solar Flares (Postprint)	
	5b. GRANT NUMBER
	5c. PROGRAM ELEMENT NUMBER 61102F

6. AUTHOR(S)	5d. PROJECT NUMBER
E. W. Cliver, G. J. D. Petrie, and A. G. Ling	2301
	5e. TASK NUMBER PPM00005402
	5f. WORK UNIT NUMBER EF004365

7. PERFORMING ORGANIZATION NAME(S) AND ADDRESS(ES)	8. PERFORMING ORGANIZATION REPORT NUMBER
Air Force Research Laboratory Space Vehicles Directorate 3550 Aberdeen Avenue, SE Kirtland AFB, NM 87117-5776	AFRL-RV-PS-TP-2014-0002

9. SPONSORING / MONITORING AGENCY NAME(S) AND ADDRESS(ES)	10. SPONSOR/MONITOR'S ACRONYM(S)
	AFRL/RVBXS
	11. SPONSOR/MONITOR'S REPORT NUMBER(S)

12. DISTRIBUTION / AVAILABILITY STATEMENT
Approved for public release; distribution is unlimited. (377ABW-2012-0333, dtd 20 Mar 2012)

13. SUPPLEMENTARY NOTES
Accepted for publication in Astrophysical Journal, Published 23 August 2012. Government Purpose Rights.

14. ABSTRACT
We compared time profiles of changes of the unsigned photospheric magnetic flux in active regions with those of their associated soft X-ray (SXR) bursts for a sample of $75 \geq M5$ flares well-observed by GONG longitudinal magnetographs. Sixty-six of these events had stepwise changes in the spatially-integrated unsigned flux during the SXR flares. In superposed epoch plots for these 66 events, there is a sharp increase in the unsigned magnetic flux coincident with the onset of the flare impulsive phase while the end of the stepwise change corresponds to the time of peak SXR emission. We substantiated this result with a histogram-based comparison of the timing of flux steps (onset, midpoint of step, and end) for representative points in the flaring regions with their associated SXR event time markers (flare onset, onset of impulsive phase, time of peak logarithmic derivative, maximum). On an individual event basis, the principal part of the stepwise magnetic flux change occurred during the main rise phase of the SXR burst (impulsive phase onset to SXR peak) for ~60% of the 66 cases. We find a close timing agreement between magnetic flux steps and > 100 keV emission for the three largest hard X-ray (> 100 keV) bursts in our sample. These results identify the abrupt changes in photospheric magnetic fields as an impulsive phase phenomenon and indicate that the coronal magnetic field changes that drive flares are rapidly transmitted to the photosphere.

15. SUBJECT TERMS
magnetic fields – Sun; flares – Sun; photosphere

16. SECURITY CLASSIFICATION OF:			17. LIMITATION OF ABSTRACT	18. NUMBER OF PAGES	19a. NAME OF RESPONSIBLE PERSON
a. REPORT Unclassified	**b. ABSTRACT** Unclassified	**c. THIS PAGE** Unclassified	Unlimited	16	E. W. Cliver
					19b. TELEPHONE NUMBER *(include area code)*

This page is intentionally left blank.

ABRUPT CHANGES OF THE PHOTOSPHERIC MAGNETIC FIELD IN ACTIVE REGIONS AND THE IMPULSIVE PHASE OF SOLAR FLARES

E. W. CLIVER[1], G. J. D. PETRIE[2], AND A. G. LING[3]
[1] Space Vehicles Directorate, Air Force Research Laboratory, Sunspot, NM 88349, USA
[2] National Solar Observatory, 950 North Cherry Avenue, Tucson, AZ 85719, USA
[3] Atmospheric Environmental Research, Lexington, MA 02421, USA
Received 2011 October 28; accepted 2012 July 13; published 2012 August 23

ABSTRACT

We compared time profiles of changes of the unsigned photospheric magnetic flux in active regions with those of their associated soft X-ray (SXR) bursts for a sample of 75 $\geqslant$ M5 flares well observed by Global Oscillation Network Group longitudinal magnetographs. Sixty-six of these events had stepwise changes in the spatially integrated unsigned flux during the SXR flares. In superposed epoch plots for these 66 events, there is a sharp increase in the unsigned magnetic flux coincident with the onset of the flare impulsive phase while the end of the stepwise change corresponds to the time of peak SXR emission. We substantiated this result with a histogram-based comparison of the timing of flux steps (onset, midpoint of step, and end) for representative points in the flaring regions with their associated SXR event time markers (flare onset, onset of impulsive phase, time of peak logarithmic derivative, maximum). On an individual event basis, the principal part of the stepwise magnetic flux change occurred during the main rise phase of the SXR burst (impulsive phase onset to SXR peak) for ∼60% of the 66 cases. We find a close timing agreement between magnetic flux steps and >100 keV emission for the three largest hard X-ray (>100 keV) bursts in our sample. These results identify the abrupt changes in photospheric magnetic fields as an impulsive phase phenomenon and indicate that the coronal magnetic field changes that drive flares are rapidly transmitted to the photosphere.

Key words: magnetic fields – Sun: flares – Sun: photosphere

Online-only material: color figures, figure set

1. INTRODUCTION

During the last decade, large, prompt, and permanent flare-associated changes in the line of sight or longitudinal component of photospheric magnetic fields have been reported by a number of authors (e.g., Kosovichev & Zharkova 2001; Wang et al. 2002; Spirock et al. 2002; Liu et al. 2005; Sudol & Harvey 2005; Wang 2006; Wang & Liu 2010; Petrie & Sudol 2010). As Sudol and Harvey (2005) pointed out, such changes conflict with current theories of solar flares (see Priest and Forbes 2002 for a review) in which it is assumed that photospheric magnetic fields remain unchanged during flares.

Sudol & Harvey (2005) examined the timing between flares and field changes for a sample of 15 X-class soft X-ray (SXR) events observed by Global Oscillation Network Group (GONG) longitudinal magnetometers and found that for all but one (equivocal) case the photospheric field changes occurred after the start of the flare. They concluded that the photospheric field changes were not flare triggers but rather another, not unimportant, phenomenon that accompanies solar flares. Similarly, Petrie & Sudol (2010) concluded that the longitudinal magnetic field changes they observed in a larger sample of 77 M- and X-class flares were a consequence of flares rather than a driver. This is in keeping with the standard view of flares (e.g., Forbes 2000) in which the free energy resides in coronal currents.

While Sudol & Harvey (2005) and Petrie & Sudol (2010) stressed that magnetic field changes systematically lagged behind flare onset, recent reviews (Hudson 2011; Fletcher et al. 2011), citing Sudol & Harvey (2005), emphasize a close connection between the flare impulsive phase and stepwise photospheric field changes. For example, Fletcher et al. (2011), in reference to observations of the 2001 August 25 flare reported

on by Sudol & Harvey, write: "The line-of-sight magnetic field changes abruptly at the time of the flare impulsive phase . . ."

Both Sudol & Harvey (2005) and Petrie & Sudol (2010) compared the magnetic field change time profiles with the onset of the overall flare rather than with the onset of the impulsive phase. These times can be quite different. For example, for the 2006 December 6 eruptive flare (Balasubramaniam et al. 2010), which had the largest stepwise magnetic field change in the sample of Petrie & Sudol (2010), the flare onset preceded the impulsive phase onset by ∼10 minutes. Veronig et al. (2002b) showed that on average the flare onset in SXRs precedes the onset of hard X-ray emission (a signature emission of the impulsive phase) by ∼3 minutes. Because the impulsive phase is the time of the most rapid energy release in a flare (e.g., Hudson 2011), a statistical comparison of the timing of magnetic field changes with the onset and end of this phase is warranted.

In this study, we will make such a comparison between the unsigned magnetic flux time profiles of flaring active regions and (1) flare SXR profiles for the sample of the 77 $\geqslant$ M5 SXR events from the study of Petrie & Sudol (2010) and (b) a subset of three large hard X-ray (>100 keV) events observed by the *Ramaty High-Energy Solar Spectroscopic Imager* (*RHESSI*; Lin et al. 2002). Our analysis is presented in Section 2 and the results are summarized and discussed in Section 3.

2. ANALYSIS

2.1. Data

The magnetogram data used in this analysis were obtained from the GONG network of longitudinal magnetographs (Harvey et al. 1988). Weather permitting, the six-station network provides continuous coverage; the effective duty cycle

is ∼87%. The Ni I (6768 Å) magnetographs produce a full-disk magnetogram every minute with spatial resolution of 2.5 arcsec pixel^{-1} and sensitivity of ∼3 G pixel^{-1}.

In our analysis, we used the event sample compiled by Petrie & Sudol (2010). For the period 2001 April to 2007 June, they examined 77 ⩾ M5 SXR (1–8 Å) flares (38 X-class and 39 M-class) that were located within 65° of central meridian and had data coverage beginning on the order of one hour before the flare and extending for approximately one hour after. The GONG magnetic flux measurements and data reduction are described in detail in Petrie & Sudol (2010). To identify abrupt, stepwise changes in the longitudinal field (B_l), those authors fitted to each pixel time series the function given by Sudol & Harvey (2005),

$$B_l(t) = B_{\text{lin}}(t) + B_{\text{step}}(t), \qquad (1)$$

where $B_{\text{lin}}(t) = a + bt$ and $B_{\text{step}}(t) = a + bt + c\{1 + (2/\pi)\tan^{-1}[n(t - t_0)]\}$. Here, t = time, a and b model the background field evolution, c represents the half-amplitude of the field change, t_0 represents the midpoint of the field change, and n is the inverse of the timescale over which the field change occurs. From this procedure, values for the background pre-flare field intensity (a), the background linear rate of field change (b), the half-amplitude of the abrupt, stepwise field change (c), the period of time over which the magnetic field change occurs (π/n), and the step midpoint (t_0) were derived for each pixel, accompanied by a measure of the goodness of the functional fit to the data.

While all pixels in an active region were considered in these flux determinations, Petrie & Sudol (2010) only selected pixels with the following characteristics: (1) the stepwise change ($2c$) was at least 1.4 times larger than the background noise level. (2) The measurements passed a goodness-of-fit test, i.e., a function of the form of Equation (1) was successfully fitted to the data. (3) The background field and field change values were not unreasonably large. In practice, this means that $|a| < 1000\,\text{G}$ and $2|c| < 350\,\text{G}$. On the Sun, fields stronger than 1000 G may change in an abrupt, stepwise way during flares, and stepwise changes greater than 350 G surely occur. Petrie & Sudol (2010) found, however, that for background fields stronger than 1000 G in GONG's 2.5 arcsec pixels, the noise level was too great for a reliable detection of stepwise changes to be possible in general. Furthermore, changes of >350 G tended to be compromised by transient emission artifacts in the signal that were not always caught by applying criterion (2). Thus, Petrie & Sudol (2010) visually inspected all pixels which exhibited stepwise changes >350 G and in doing so identified two notable exceptions to criterion (3). Event Nos. 55 and 75 in Table 1 both exhibited stepwise field changes of ∼450 G. (4) The field change was complete within 40 minutes. We are only interested in abrupt field changes as opposed to steady background evolution.

In applying selection criteria (1)–(4), care was taken to filter transient artifacts in the data (e.g., Patterson 1984; Kosovichev & Zharkova 2001; Qiu & Gary 2003) and to select only real field-change signatures. Because any flare can involve hundreds or thousands of pixels that may have caught genuine flare-related field changes, this selection process is automated. Petrie & Sudol (2010) carried out two parallel statistical studies: one using the automated pixel selection procedure employed in the present paper and one using a much more selective procedure, where only a few manually chosen pixels showing the largest, most abrupt field changes with the highest signal-to-noise ratios were used. The two statistical studies produced consistent results.

Since we are considering the unsigned flux, it will always increase by definition. It is important to note, however, that in the signed data, flux changes tend to be negative (Petrie & Sudol, 2010).

Figures 1(a) and (b) illustrate the data used in our analysis for two events with large flux steps. The top panel of this figure contains the time profiles of the spatially integrated (over the selected pixels) unsigned magnetic flux changes (in black; with mean subtracted) and the associated SXR time profile (red). The solid red vertical lines in the top panel give the flare onset and peak times. The SXR burst onset time is determined from a sequence of four one minute averages meeting the following requirements: (1) all points must be ⩾$1 \times 10^{-7}\,\text{W m}^{-2}$ (B-class), (2) the intensity must monotonically increase, and (3) the intensity of the fourth point must be >1.4 times the intensity of the first point.

The dashed red lines in Figure 1 correspond to the onset of the flare impulsive phase as determined by the logarithmic derivative in the bottom panel. We designated this time to be the minute during which the average SXR flux increased by ⩾40% from the average for the previous minute, with the additional requirement that the logarithmic derivative stays above this 40% level until it reached its maximum value in the event. This requirement addressed 12 cases where an early peak in the derivative (dashed blue line in the event plots) was followed by a drop below the 40% level and a later larger peak. Other levels than 40% can be used; e.g., Cliver et al. (2004) required a minute-to-minute increase of ∼100%. But even large (⩾M5) SXR flares may not exhibit a minute-to-minute increase of 40%, let alone 100%. In the nine such cases in our sample, we used the time of the peak derivative as the onset of the impulsive phase. Figures in the same format as Figure 1 are given in the Electronic Supplement for all 77 events in our data sample.

The parameters for the 77 events are listed in Table 1. The basic event data—date, SXR onset time, SXR flare class, and Hα flare location—are given in Columns 2, 3, 5, and 6, respectively. Column 4 shows that the onset of the impulsive phase in SXRs follows the flare onset by a median value of 3 minutes (range from 1 to 59 minutes; mean of 6.9 minutes). The seven events with delays >15 minutes are complex events with one or more peaks and/or plateaus. Column 7 gives the coronal mass ejection (CME) association for each flare (Y = yes; N = no) taken from the *Solar and Heliospheric Observatory* (*SOHO*) Large Angle Spectroscopic Coronagraph (Brueckner et al. 1995) CME Catalog (Yashiro et al. 2004). Several events have "Unc." (= uncertain) listed in these columns based on the assessment in the list compiled by Yashiro et al. (2006) that a CME could not be confirmed or ruled out for these cases. Column 8 contains the step midpoint (t_0) and Column 9 contains the step duration (Δt) for the "representative" point with the largest flux change identified by Petrie & Sudol (2010) for each flare. Representative points are averages of 4 pixels "that approximate the most abrupt and the most significant change in the magnetic field" (Sudol & Harvey (2005). Notes for individual events are given in Column 10. We did not use event Nos. 61 (widely varying magnetic flux profile prior to the flare) and 68 (missing flux data at flare peak) in our analysis, reducing our sample to 75 events.

2.2. Timing Comparison of Magnetic Flux Change and Soft X-Ray Flare Impulsive Phase

Figures 2(a) and (b) contain superposed epoch plots of the magnetic flux profiles for the 75 events in our sample, with the time of zero epoch corresponding to the onset of the

Table 1
Parameters of the Analyzed Flares

Number	Date[a]	SXR Flare Onset	Delay to Imp. Phase	SXR Flare Class	Hα Flare Location	CME?[b]	t_0	Δt	Notes[c]
	(mm/dd/yyyy)	(UT)	(minutes)				(UT)	(minutes)	
(1)	(2)	(3)	(4)	(5)	(6)	(7)	(8)	(9)	(10)
1	**04/02/2001**	21:31	7	X18.4	N18W65	Y	21:43:29	1.0	1,2
2	06/22/2001	22:14	2	M6.7	N14W47	Unc.	22:24:41	14.8	
3	06/23/2001	00:10	1	M5.9	N09E24	N	00:19:49	25.8	
4	*06/23/2001*	04:02	2	X1.3	N10E23	N	04:17:42	25.8	3
5	**08/25/2001**	16:23	4	X5.7	S17E34	Y	16:41:25	22.5	
6	09/05/2001	14:25	2	M6.4	N15W31	N	14:30:42	17.5	
7	09/09/2001	20:40	2	X1.0	S31E26	N	20:48:43	5.2	
8	**09/16/2001**	03:39	6	M6.1	S29W54	Unc.	03:45:55	4.3	
9	**10/19/2001**	16:13	9	X1.7	N15W30	Y	16:32:25	28.0	2
10	*10/22/2001*	14:27	3	M6.9	S21E18	Y	14:35:05	25.8	4
11	**10/22/2001**	17:44	6	X1.2	S18E16	Y	17:49:50	8.2	
12	***10/23/2001***	02:11	3	M7.0	S18E11	N	02:15:29	1.0	
13	**11/07/2001**	19:30	2	M5.9	S17E44	D.G.	19:35:05	13.9	5
14	**11/08/2001**	06:59	2	M9.7	S19W19	D.G.	07:03:01	4.1	
15	*11/28/2001*	16:26	6	M7.2	N04E16	Y	16:36:26	4.3	
16	11/29/2001	10:12	8	M5.8	N04E10	Unc.	10:22:14	11.3	5
17	12/11/2001	07:58	3	X2.9	N16E41	Y	08:11:51	26.1	
18	*12/26/2001*	04:32	32	M7.6	N08W54	Y	04:51:55	21.6	4
19	**01/09/2002**	17:42	3	M9.9	N13W02	Unc.	17:48:28	1.0	
20	**03/14/2002**	01:38	2	M6.0	S12E23	N	01:46:14	20.5	
21	05/20/2002	15:21	2	X2.1	S21E65	Y	15:34:06	6.1	
22	**07/11/2002**	14:43	2	M5.9	N21E56	Y	14:55:54	29.5	
23	**07/17/2002**	06:58	2	M9.0	N20W16	Y	07:13:29	25.7	
24	07/26/2002	20:50	12	M9.1	S19E26	Y	21:09:43	22.2	4
25	***08/16/2002***	11:32	2	M5.4	S14E20	Y	11:46:38	32.5	4
26	*08/20/2002*	01:33	4	M5.5	S10W35	Y	01:44:15	2.1	2
27	08/21/2002	05:28	2	X1.0	S10W51	Y	05:42:25	34.1	
28	10/05/2002	20:42	10	M6.3	N14E31	Y	20:49:35	6.0	
29	11/18/2002	02:01	2	M7.6	S16E56	N	02:06:21	12.0	
30	12/20/2002	13:12	2	M7.3	S26W32	N	13:23:30	31.1	
31	*03/17/2003*	18:50	6	X1.7	S14W38	Y	19:09:35	37.2	
32	**03/18/2003**	11:51	3	X1.6	S13W46	Y	11:59:16	1.0	
33	**05/27/2003**	22:56	2	X1.4	S06W20	Y	22:59:01	4.5	
34	**05/28/2003**	00:17	2	X3.9	S06W20	Y	00:22:29	1.0	
35	*06/10/2003*	23:19	38	X1.4	N14W50	D.G.	23:32:21	7.3	2,5
36	**06/11/2003**	20:00	4	X1.8	N14W57	D.G.	20:18:05	36.8	
37	**10/19/2003**	16:29	5	X1.1	N08E58	Y	16:45:17	10.8	
38	**10/26/2003**	05:57	12	X1.3	S16E40	Y	06:16:31	10.3	5
39	*10/26/2003*	17:21	9	X1.3	N02W38	Y	17:21:29	21.0	4
40	***10/26/2003***	21:34	2	M8.3	N01W38	Unc.	21:41:13	18.7	
41	**10/27/2003**	09:20	2	M5.3	S15E26	Unc.	09:23:23	8.7	
42	**10/29/2003**	20:37	2	X10.8	S15W02	Y	20:41:29	1.0	
43	**11/02/2003**	17:03	12	X9.2	S14W56	Y	17:21:27	26.5	
44	11/20/2003	07:35	2	X1.0	N01W08	Y	07:38:25	1.0	
45	***11/20/2003***	23:42	3	M6.1	N02W17	Y	00:00:40	15.6	
46	***01/17/2004***	17:35	7	M5.2	S15E19	Y	17:50:02	5.7	1,2
47	**01/20/2004**	07:29	2	M6.5	S16W12	Y	07:41:59	33.4	
48	*02/26/2004*	01:50	2	X1.2	N14W15	N	02:04:30	26.1	3
49	**07/13/2004**	00:09	2	M7.3	N14W45	Y	00:22:16	24.3	1
50	**07/13/2004**	19:24	4	M6.7	N14W56	Y	19:30:28	1.0	2
51	*07/15/2004*	01:30	6	X1.9	S10E34	Y	01:45:03	28.2	1
52	*07/15/2004*	18:14	6	X1.7	S11E45	N	18:15:44	2.8	1,2,3
53	07/16/2004	01:43	18	X1.4	S11E41	N	02:00:30	27.4	1,3
54	*07/16/2004*	10:32	4	X1.1	S10E36	N	10:43:58	38.8	2,3
55	**07/16/2004**	13:49	2	X3.8	S09E32	N	14:04:42	35.6	3
56	**07/20/2004**	12:22	2	M8.9	N10E33	Y	12:33:12	28.5	
57	***07/22/2004***	00:14	6	M9.5	N03E17	Y	00:28:23	38.9	1,4
58	07/25/2004	05:39	3	M7.6	N10W31	Y	05:57:24	38.8	
59	08/13/2004	18:07	1	X1.1	S13W23	Y	18:25:22	39.1	
60	08/14/2004	05:36	4	M8.0	S13W29	N	05:47:42	21.9	
61	10/30/2004	11:38	3	X1.3	N11W26	Y	11:53:38	17.7	1,6
62	10/30/2004	16:18	3	M6.2	N13W28	Y	16:35:18	37.5	5
63	01/01/2005	00:01	24	X1.8	N06E34	Y	00:20:36	39.8	1,2,5

3

Table 1
(Continued)

Number	Date[a]	SXR Flare Onset	Delay to Imp. Phase	SXR Flare Class	Hα Flare Location		t_0	Δt	Notes[c]
	(mm/dd/yyyy)	(UT)	(minutes)			CME?[b]	(UT)	(minutes)	
(1)	(2)	(3)	(4)	(5)	(6)	(7)	(8)	(9)	(10)
64	*01/15/2005*	00:22	16	X1.3	N11E10	N	00:33:33	15.4	2,3,5
65	01/15/2005	04:26	2	M8.9	N11E08	N	04:39:46	10.9	
66	***01/15/2005***	05:54	2	M9.1	N11E06	Y	06:06:23	30.6	4
67	**01/15/2005**	22:25	7	X2.8	N14W08	Y	22:44:20	29.3	4
68	01/17/2005	06:59	55	X4.1	N14W24	Y	07:07:06	3.2	5,6
69	**01/20/2005**	06:36	4	X7.9	N12W58	Y	06:43:30	1.0	
70	**07/30/2005**	06:17	3	X1.3	N11E59	Y	06:25:23	6.2	
71	***09/10/2005***	16:34	3	X1.2	S11E47	Unc.	16:39:09	15.6	1
72	***09/10/2005***	21:30	3	X2.2	S13E47	Y	21:34:42	10.6	4
73	***09/13/2005***	19:19	2	X1.5	S09E10	Y	19:22:17	1.0	
74	***12/06/2006***	08:02	12	M6.0	S06E63	D.G.	08:21:45	37.3	2
75	**12/06/2006**	18:29	11	X6.5	S06E63	Rmnts.	18:43:22	2.6	7
76	12/14/2006	21:06	59	X1.6	S06W46	Y	21:15:43	12.6	1,2
77	06/04/2007	05:06	2	X1.0	S07E51	N	05:23:28	19.5	

Notes.

[a] Dates in bold/underlined font indicate events for which the bulk (two-thirds or more) of the abrupt rise in the unsigned flux occurs within the confines of the flare impulsive phase (adding a minute on either side because of the noise in the data). Dates in italics indicate events with small step changes $\lesssim 3 \times 10^{19}$ Mx.

[b] Y, yes; N, no; Unc., uncertain association; D.G., LASCO data gap.

[c] Notes in Column 10: (1) no flare patrol (or no flare reported; No. 72); (2) earlier peak in logarithmic derivative $\geqslant 1.4$; (3) X-class CME-less event (Gopalswamy et al. 2009; Wang & Zhang 2007); (4) logarithmic derivative < 1.4; (5) one (or more) $\geqslant$ M1 peaks in the SXR profile preceded the maximum listed in Column 5; (6) not used in the analysis because of uncertain or incomplete magnetic flux data; (7) CME remnants observed after data gap (Balasubramaniam et al. 2010).
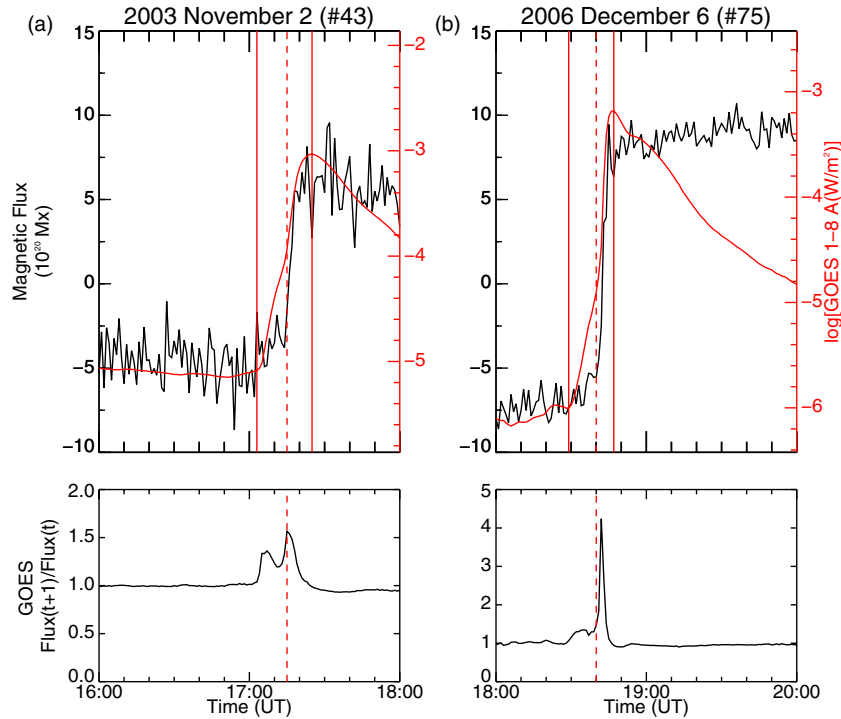
Figure 1. (a) Top: time profiles of the spatially integrated unsigned magnetic flux in the flaring region (black line, with mean subtracted) and the 1–8 Å intensity (red line) of the X8.3 soft X-ray (SXR) flare on 2003 November 2. The solid red lines mark the start and peak times of the SXR burst and the dashed red line indicates the onset of the flare impulsive phase. The SXR intensity axis covers four magnitudes and has been adjusted so that the 1–8 Å intensity tracks the magnetic flux profile prior to the flare. The number of the event in Table 1 is given at the top of the figure. Bottom: the minute-to-minute logarithmic derivative of the flare SXR intensity. The onset of the flare impulsive phase (as defined in the text) is indicated by a dashed red line. (b) Same as (a) for the X6.5 flare on 2006 December 6. The Electronic Supplement contains plots in the same format as (a) and (b) for all 77 events in Table 1.

(The complete figure set (77 images) is available in the online journal)
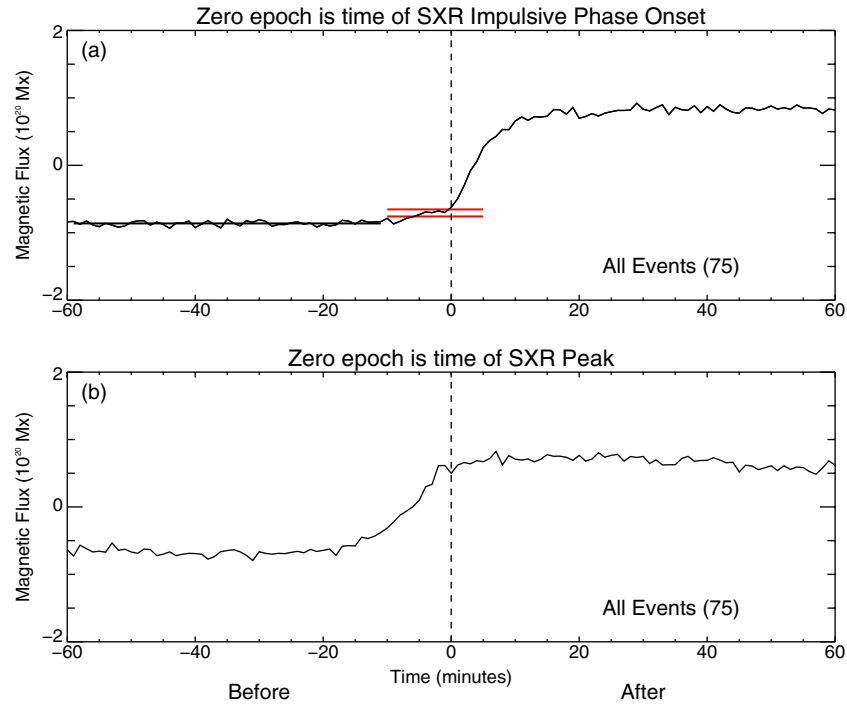
Figure 2. (a) Superposed epoch plot of the unsigned magnetic flux variation in a flaring region measured by GONG magnetographs for 75 events in Table 1 (excluding event Nos. 61 and 68 (see the text)); zero epoch corresponds to the onset of the flare impulsive phase in SXRs. The black horizontal line is the mean of the trace for the interval from 60 minutes to 10 minutes before the time of zero epoch and the red lines are drawn 3σ and 6σ above the mean from -10 minutes to $+5$ minutes relative to zero epoch. (b) Same as (a), except in this case zero epoch corresponds to the peak of the SXR emission. The number of events used to make the superposed epoch plots are given in parentheses.

(A color version of this figure is available in the online journal.)

flare impulsive phase in SXRs and the peak SXR emission, respectively. Upward trends in the superposed epoch plots (that can be seen in approximately half of the individual plots in the Electronic Supplement, e.g., Nos. 4, 12, 23, 30, 59, 71, and 73) were removed by fitting a straight line to the flux data before the flare onset and rotation of the plotted data about a pivot point. This was done by repeated linear fits of the data between 60 minutes before zero epoch and an upper limit that was allowed to vary from 20 to 0 minutes before zero epoch in one minute steps. The Pearson correlation coefficient was computed between the data and the results of the fit for each iteration of the upper time limit. The pivot point was taken to be the minute before the time at which the correlation coefficient decreased when the upper time limit was increased. Then all two hours of the data were rotated about this point to change the slope of the line determined from the fit results to zero. These composite profiles confirm the impression given by Figure 1—specifically, that the principal abrupt flux changes begin near the onset of the flare impulsive phase and end near the time of peak SXR emission. In Figure 2(a), the black horizontal line is the mean flux value over the interval from 60 minutes to 10 minutes prior to zero epoch and the red horizontal lines are drawn 3σ (standard deviations) and 6σ above this mean. The magnetic flux time profile remains $>6\sigma$ above the pre-event mean for times > 0.

Inspection of the plots in the Electronic Supplement reveals nine events (Nos. 3, 6, 16, 28, 29, 53, 63, 65, and 76) that lack permanent step changes during the SXR flare. Consistent with the big flare syndrome (Kahler 1982), the nine flares without magnetic flux steps were less energetic than the 66 events that exhibited stepwise changes (mean peak SXR class of M9.9 versus X2.0). In addition, the nine events were less likely to

have associated CMEs (44% versus 75%; with uncertain events counted as one-half). While such events are detectable in flux plots made for representative points (Petrie & Sudol, 2010), summing over the stepwise pixel field changes that pass the selection criteria outlined in Section 2.1 can obscure small localized changes, resulting in a composite flux profile without a clearly discernible step, as was the case for these nine events.

Figure 3 is a repeat of Figure 2 for the reduced data set of 66 events. As expected, the amplitude of the stepwise flux change is larger than that in Figure 2. Figure 4 is a repeat of Figures 2 and 3 for the smallest third (22/66) of the events in the sample; these events, with step changes $\lesssim 3 \times 10^{19}$ Mx, are indicated by italicized dates in Table 1. While the step amplitude in Figure 4 is significantly reduced (note that the y-axis scale is increased by a factor of four over that in Figures 2 and 3), the statistical timing relationship between the magnetic flux change and SXR intensity variation can be seen for the smallest events. In fact, there is a residue of this relationship in a superposed epoch plot (not shown) for the nine events that lacked clear steps in their unsigned magnetic flux.

Visual inspection of the individual event plots in the Electronic Supplement shows that for 41 of the 66 events (62%), the bulk (two-thirds or more) of the abrupt rise in the unsigned flux occurs within the confines of the flare impulsive phase (adding a minute on either side because of the noise in the data). These 41 events are indicated by underlined/bold dates in Table 1. The 25 exceptions included events for which the step began in association with an earlier smaller peak in the derivative, often near the SXR flare onset (e.g., Nos. 18 and 35), events for which the unsigned flux profile continued to rise after the SXR peak (e.g., Nos. 2, 17, and 77), and one very impulsive event (No. 21) for which the step change began near the peak of the SXR flare.

5
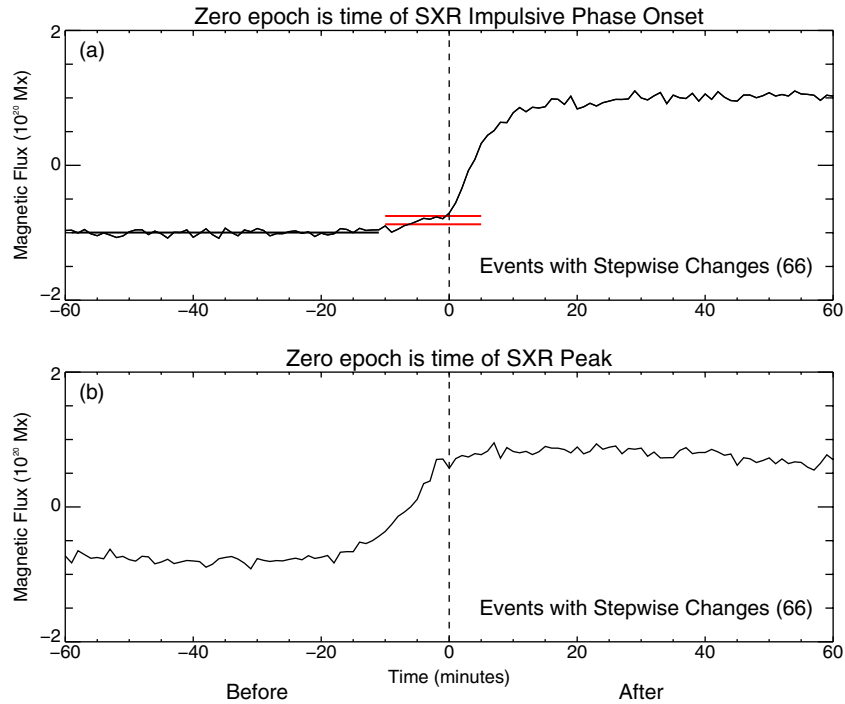
Figure 3. (a) Superposed epoch plot of the unsigned magnetic flux variation in a flaring region measured by GONG magnetographs for the 66 events in Table 1 that exhibited stepwise changes in this parameter during the associated flare; zero epoch corresponds to the onset of the flare impulsive phase in SXRs. The black horizontal line is the mean of the trace for the interval from 60 minutes to 10 minutes before the time of zero epoch and the red lines are drawn 3σ and 6σ above the mean from -10 minutes to $+5$ minutes relative to zero epoch. (b) Same as (a) except in this case zero epoch corresponds to the peak of the SXR emission. The number of events used to make the superposed epoch plots are given in parentheses.

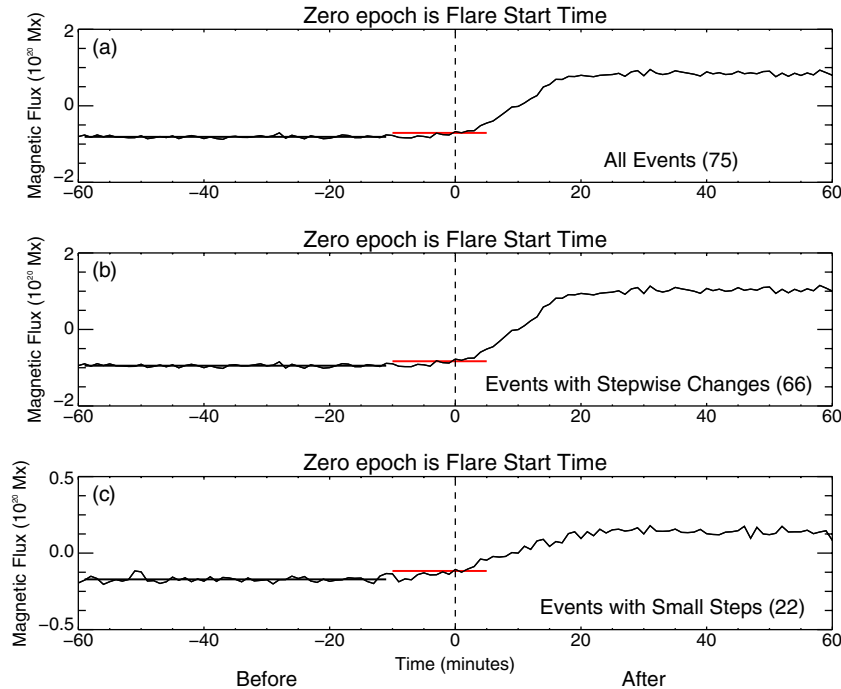(A color version of this figure is available in the online journal.)
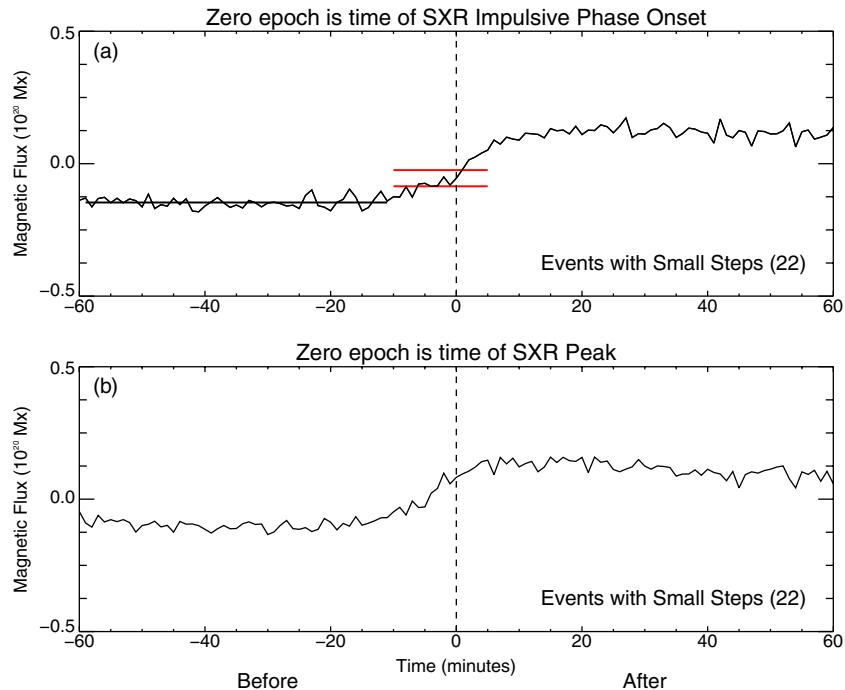
Figure 4. Same as Figures 2 and 3, but with an expanded y-scale, for the smallest third of the 66 events with stepwise flux changes.

(A color version of this figure is available in the online journal.)

2.3. Timing Comparison of Magnetic Flux Change and SXR Flare Onset

Figure 5 contains superposed epoch analyses for the three groups of events we have considered (all 75, the 66 with step changes, and the 22 with the smallest step changes), with the flare onset time, rather than the onset of the impulsive phase, used as the time of zero epoch. Note that for each sample, there is an increase in the unsigned flux beginning about five minutes before the time of zero epoch and that the signal rises

Figure 5. Superposed epoch plots of the unsigned magnetic flux, with zero epoch corresponding to the SXR flare start time, for (a) all 75 events in Table 1, (b) the subset of 66 events that had discernible stepwise flux changes, and (c) a subset of 22 events from (b) that had the smallest flux changes of the 66 events (plotted on an expanded y-scale). The red horizontal lines are drawn at 3σ above the black horizontal lines that represent the pre-event mean flux data.
(A color version of this figure is available in the online journal.)

3σ (horizontal red line) above the pre-event background near the time of the SXR flare onset and then is flat or slowly rising for a few minutes thereafter before the sharp rise at the onset of the flare impulsive phase. Examples of precursor-type activity prior to the principal step in the magnetic flux can be seen in the two large events in Figure 1.

### 2.4. Timing Analysis Based on Representative Points

To substantiate the above results, we present here an analysis based on flux steps observed in representative points identified by Petrie & Sudol (2010). Petrie & Sudol (2010) obtained the timing of the magnetic flux step in each of these representative points (Columns 8 and 9 in Table 1) that can be compared directly with flare time markers. Figure 6 contains three stacked histograms of SXR flare times (onset, impulsive phase onset, time of peak logarithmic derivative, and maximum, in descending order) relative to the (a) onset ($t_0 - (\Delta t/2)$), (b) midpoint (t_0), and (c) end of the magnetic flux step ($t_0 + (\Delta t/2)$), where Δt is the step duration. In this analysis, we only considered the 66 events with discernible flux steps in the composite flux data.

The results in Figure 6 are generally consistent with those determined from the superposed epoch analysis of the composite flux profiles in Figures 2–4. Figure 6(a) shows that the onset of the step in magnetic flux is best aligned with that of the onset of the SXR impulsive phase and Figure 6(c) shows that the end of the flux step is roughly centered on the time of SXR maximum, with a broad scatter. Figure 6(b) shows that the time of the SXR peak is better organized by the midpoint of the magnetic step. At first glance, this contradicts the results of Figures 2–4 where the SXR peak corresponds to the full amplitude (rather than the half-amplitude) of the magnetic step. Figure 7, however, shows that the ratio of the unsigned spatially integrated open magnetic flux at the time of the SXR peak to the magnetic flux at the end of the flux step ($t_0 + (\Delta t/2)$)

is skewed toward values >0.5, with a median value of >0.8. To determine these ratios, we used three-point smoothing (1/4, 1/2, 1/4) of the flux data and subtracted the flux at the step onset ($t_0 - (\Delta t/2)$) from the flux values at SXR peak and step end. Hatching in the largest bin (0.9–1) represents ratios >1 and those in the smallest bin (0–0.1) represents negative values resulting from background subtraction. We stress that while the statistical results obtained from the superposed epoch analysis of Figures 2–4 and the histogram analysis of Figures 6 and 7 are generally consistent, the behavior of step changes in B in a given representative point can differ significantly from that of integrated unsigned flux changes over an active region.

2.5. Timing Comparison of Magnetic Flux Change and Flare Hard X-Ray Emission

In Figure 8, we show that the onset of the impulsive phase obtained by taking the derivative of the SXR emission is in general agreement with the rapid rise of *RHESSI* > 100 keV emission for the three events in our sample that had peak counting rates of $>10^3$ counts s^{-1}. The *RHESSI* time profile of a fourth event with a peak count rate $>10^3$ counts s^{-1} (event No. 42; 2003 October 29) was affected by particle contamination (A. Shih 2011, private communication) and was not considered. On the plots, we have indicated the time of SXR flare onset (solid red line) and the onset of the SXR impulsive phase (dashed red line). For the 2003 November 2 event, the onset of the impulsive phase in SXRs matches that in >100 keV X-rays while for the other two events, the SXR impulsive phase onset precedes that in >100 keV X-rays by about two minutes. In all three cases, the onset of the sustained rise in the unsigned magnetic flux time profile is coincident with, or precedes, the onset of the sharp rise in >100 keV emission.

7
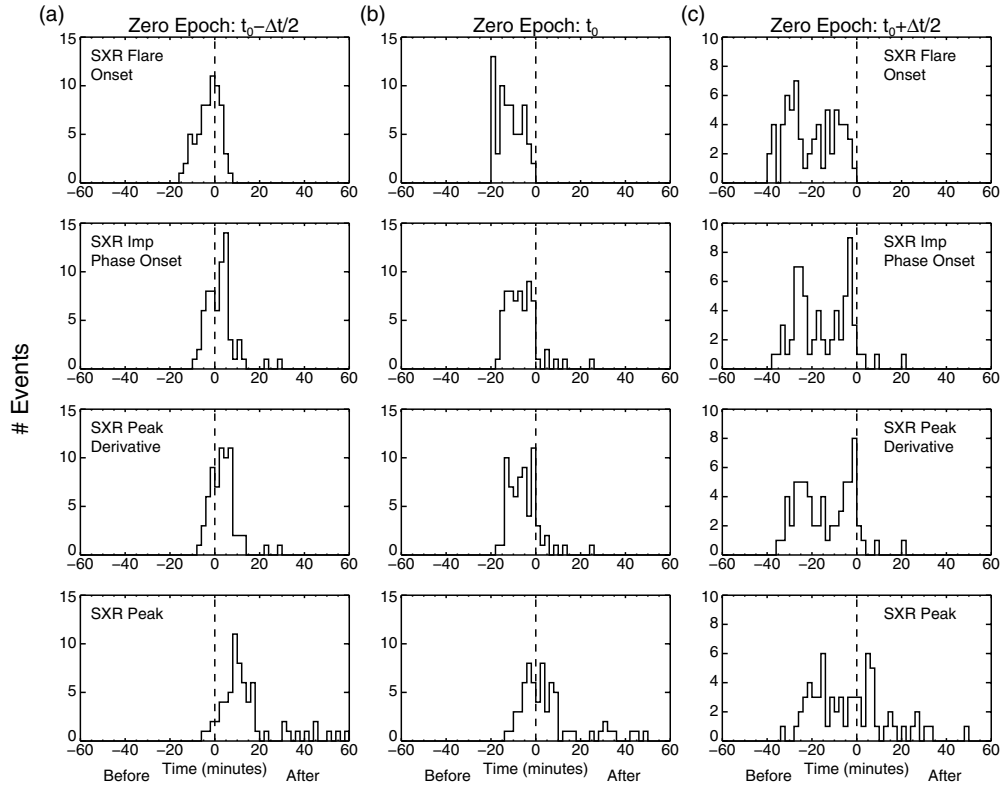
Figure 6. Timing of SXR flare markers (onset, impulsive phase onset, time of peak logarithmic derivative, and peak) relative to (a) the onset ($t_0 - (\Delta t/2)$) of the step in B for the representative pixel with the largest field change for each of the 66 events that exhibited such stepwise field changes, (b) the midpoint (t_0) of the flux step, and (c) the end time ($t_0 + (\Delta t/2)$) of the step.
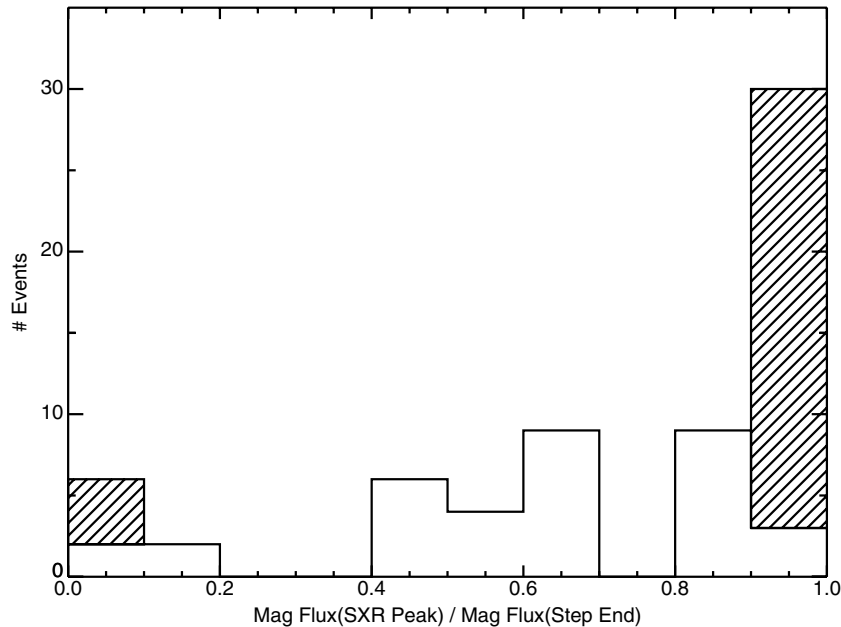

Figure 7. Histogram for the ratio of the spatially integrated unsigned magnetic flux at the peak of the SXR flare to the flux at the end ($t_0 + (\Delta t/2)$) of the magnetic step. Hatching in the largest bin (0.9–1) represents ratios >1 and those in the smallest bin (0–0.1) represents negative values resulting from background subtraction.

3. SUMMARY AND DISCUSSION

We investigated the timing relationship between step changes in the unsigned magnetic flux in active regions and associated flare SXR emission for a sample of 75 ⩾ M5 SXR flares taken from Petrie & Sudol (2010). Sixty-six of these events exhibited stepwise magnetic flux changes. A superposed epoch analysis

of the spatially integrated flux changes in these events showed that, on average, the flux change rose sharply at the onset of the SXR flare impulsive phase and ended near the peak of the SXR event (Figures 2–4). A separate analysis based on the timings of the flux steps in representative points in the flaring regions for the 66 events (Figures 6 and 7) substantiated these results. The temporal correspondence of the stepwise change in the unsigned
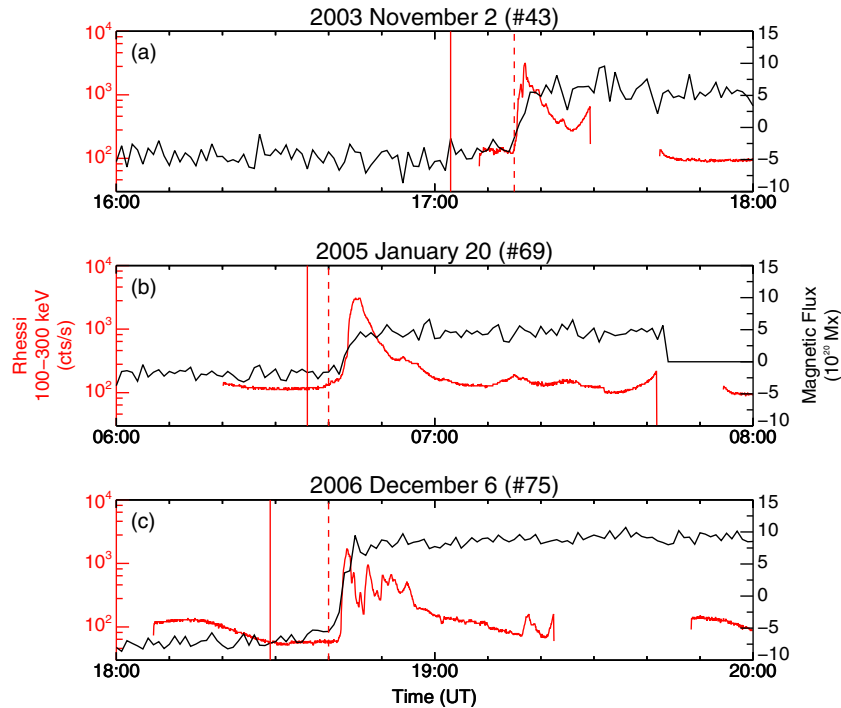
Figure 8. *RHESSI* 100–300 keV time profiles (red trace) and unsigned magnetic flux variation (black trace) for large flares on (a) 2003 November 2, (b) 2005 January 20, and (c) 2006 December 6. The solid and dashed red lines indicate the SXR flare start time and the onset of the impulsive phase (as determined in SXRs), respectively.

flux and the flare impulsive phase is also observed for a subset of three large >100 keV events (Figure 8). We conclude that abrupt longitudinal magnetic field changes in the photosphere are a phenomenon of the flare impulsive phase.

Comparison of the SXR and magnetic flux profiles for the 66 events in our sample with detectable magnetic flux changes reveals that in ~60% of these cases, the principal part of the step changes in the unsigned flux occurred during the flare impulsive phase. For comparison with other phenomena identified with the flare impulsive phase, we note that Maričić et al. (2007) found that the main acceleration phase of CMEs (Zhang et al. 2001) was synchronized with the SXR rise 50%–75% of the time (sample size of 22 events), while Veronig et al. (2002a) found that about half of the 1114 events they examined exhibited a timing behavior that was consistent with the Neupert effect (Neupert 1968; Dennis & Zarro 1993).

Previously, both Sudol & Harvey (2005) and Petrie & Sudol (2010) reported that photospheric flux changes characteristically follow the SXR flare onset. This result is unchanged. In the superposed epoch plot of Figure 5, we do not see a sustained significant (3σ) increase in the unsigned flux before the flare start time, although there is a suggestion of low-level flux increase beginning about five minutes prior to flare onset. We note that in about 30% of the 77 events analyzed by Petrie & Sudol (2010), magnetic flux changes preceded the SXR flare onset but these flux changes were discounted as an artifact of the model used to fit the step changes.

Our finding that magnetic flux steps in solar flares are an impulsive phase phenomenon can be inferred from Figure 3 in Sudol & Harvey (2005) based on a smaller sample of 15 X-class events. That figure shows that in the bulk (10) of their events, the magnetic step in *B* in a representative point began after flare onset and ended close to flare maximum. It is instructive to examine a few of the events where that did not happen. For the 2001 October 19 event (No. 9 in Table 1), the SXR peak occurs

near the middle of the step in *B*. In the plot of the change in the spatially integrated flux (Figure 9 in the Electronic Supplement), however, it can be seen that the principal part of the step has been completed by the time of the SXR maximum, and the subsequent rate of change is much slower than that beginning near the onset of the impulsive phase. A similar example of this behavior can be seen in Electronic Supplement Figure 36 for the Sudol & Harvey event on 2003 June 11. These cases show that magnetic steps in representative points, while generally similar to the steps in the spatially integrated unsigned flux we have considered here, can differ significantly for certain cases. For the event of 2003 October 26 (start at 05:57 UT), the plot in Sudol and Harvey (2005) shows that the SXR peak occurs well after the step in *B* has ended. For this event (No. 38 in Table 1), Plot 38 in the Electronic Supplement shows that the step in *B* occurred in conjunction with an earlier X-class peak in a blended event.

In our (initial) sample of 77 events (Table 1), the impulsive phase lagged the flare onset by a median of three minutes. Thus, by focusing on the onset of the impulsive phase, which signals the most energetic phase of the flare (e.g., Zhang et al. 2001, Hudson 2011), we move the flare time marker closer to the abrupt change in the longitudinal field. Wang & Liu (2010) recently examined line-of-sight field changes in 18 events (6 in common with our sample) observed with 1 minute cadence by the Michelson Doppler Imager (Scherrer et al. 1995) on *SOHO*. Their study did not focus on the relative timing of the flux changes and flare light curves and they remark, with some ambiguity, that in all cases the flux changes were "co-temporal with the flare initiation." Their Figure 2, however, shows a close correspondence between the onsets of rapid magnetic flux change and the impulsive phase of SXR flare emission in the X-class flare on 2001 September 24.

Both Sudol & Harvey (2005) and Petrie & Sudol (2010) considered the flux changes to most likely be due to changes

9

in field direction rather than intensity. Petrie and Sudol (2010) simulated the variation of line-of-sight field strength with solar longitude (viewing angle) and compared their results with observed changes within the $\pm 65°$ (measured from disk center) longitudinal range of their events. They found a tendency for the observed line-of-sight fields to decrease during flares near disk center, indicating that the field had become more horizontal. Similarly, Wang & Liu (2010), from a vector magnetograph study of 11 X-class flares (3 in common with our sample), found that the transverse field at the polarity inversion line always increased. More recently, several authors (Wang et al. 2012; Gosain 2012; Sun et al. 2012; Petrie 2012) used data from the Helioseismic and Magnetic Imager (HMI; Schou et al. 2012) on *Solar Dynamics Observatory* (*SDO*) to present evidence of an enhancement of transverse magnetic field at the flaring magnetic polarity inversion line for an X2.2 flare on 2011 February 15.

This propensity for active region magnetic fields to become more horizontal during flares is consistent with the magnetic "implosions" conjectured by Hudson (2000; see Hudson & Cliver 2001, Liu & Wang 2010, and Hudson 2011 for schematics of this process) to power the impulsive phase of flares (Hudson et al. 2008). While such field line "shrinkage" is observed in the late phase of flares (Švestka et al. 1987; Forbes & Acton 1996; Mckenzie & Hudson 1999) and is thought to supply the energy for post-eruption loop formation, the Hudson conjecture specifically refers to the impulsive phase when the energy release rate reaches its maximum and CMEs undergo their main acceleration. Direct evidence for such field line implosion at the peak of an X-class on 2005 September 8 was reported by Liu & Wang (2010). *Transition Region and Coronal Explorer* (Handy et al. 1999) images at 171 Å showed retraction of a coronal loop from a height of $\sim 10^5$ km above the flaring region beginning about four minutes after the onset of the flare impulsive phase. Liu & Wang suggest that the delayed onset of the fast contraction reflects propagation at an average rate of ~ 500 km s^{-1} of the coronal magnetic instability responsible for the flare. These authors also reported loop retraction during the impulsive phase for an M-class flare on 2004 July 20 observed, at 12 minute cadence, by the Extreme-ultraviolet Imaging Telescope (Delaboudinière et al. 1995) on *SOHO*. Recently, Gosain (2012) presented 171 Å images from the Atmospheric Imaging Assembly (Lemen et al. 2012; Boerner et al. 2012) on *SDO* of the collapse of low lying loops during the flare impulsive phase of the well-studied X-class flare on 2011 February 15. For the same event, Petrie (2012) reported an HMI-based increase in total field strength near the neutral line and calculated an abrupt downward Lorentz force change there at the time of the flare, strengthening the case for Hudson's implosion/loop contraction scenario.

The flare impulsive phase marks the period of rapid conversion of energy stored in coronal magnetic fields into particle acceleration and plasma heating (Neupert, 1968) as well as mass motion (Zhang et al. 2001). The timing agreement we find between the impulsive phase and the stepwise change of the unsigned longitudinal magnetic flux (Figures 2–4, 6, and 8) indicates, at a minimum, that the coronal field restructuring responsible for flares is rapidly transmitted to the photosphere (Emslie & Sturrock 1982; Fletcher & Hudson 2008; Wang & Liu 2010, Hudson et al. 2011). As a more basic—and speculative—inference, the strong abrupt photospheric field changes observed during the flare impulsive phase may be evidence of magnetic implosions.

REFERENCES

Balasubramaniam, K. S., Cliver, E. W., Pevtsov, A., et al. 2010, ApJ, 723, 587
Boerner, P., Edwards, C., Lemen, J., et al. 2012, Sol. Phys., 275, 41
Brueckner, G. E., Howard, R. A., Koomen, M. J., et al. 1995, Sol. Phys., 162, 357
Cliver, E. W., Nitta, N. V., Thompson, B. J., & Zhang, J. 2004, Sol. Phys., 225, 105
Delaboudinière, J.-P., Artzner, G. E., Brunaud, J., et al. 1995, Sol. Phys., 162, 291
Dennis, B. R., & Zarro, D. M. 1993, Sol. Phys., 146, 177
Emslie, A. G., & Sturrock, P. A. 1982, Sol. Phys., 80, 99
Fletcher, L., Dennis, B. R., Hudson, H. S., et al. 2011, Space Sci. Rev., 159, 19
Fletcher, L., & Hudson, H. S. 2008, ApJ, 675, 1645
Forbes, T. 2000, J. Geophys. Res., 105, 23153
Forbes, T. G., & Acton, L. W. 1996, ApJ, 459, 330
Gopalswamy, N., Akiyama, S., & Yashiro, S. 2009, in IAU Symp. 257, Universal Heliophysical Processes, ed. N. Gopalswamy & D. F. Webb (Cambridge: Cambridge Univ. Press), 283
Gosain, S. 2012, ApJ, 749, 85
Handy, B. N., Acton, L. W., Kankelborg, C. C., et al. 1999, Sol. Phys., 187, 229
Harvey, J., Abdel-Gawad, K., Ball, W., et al. 1988, in Seismology of the Sun and Sunlike Stars, ed. E. J. Rolfe (ESA SP-286; Noordwijk: ESA), 203
Hudson, H. S. 2000, ApJ, 531, L75
Hudson, H. S. 2011, Space Sci. Rev., 158, 5
Hudson, H. S., & Cliver, E. W. 2001, J. Geophys. Res., 106, 25199
Hudson, H. S., Fisher, G. H., & Welsch, B. T. 2008, in ASP Conf. Ser. 383, Subsurface and Atmospheric Influences on Solar Activity, ed. R. Howe et al. (San Francisco, CA: ASP), 221
Kahler, S.W 1982, J. Geophys. Res., 87, 3439
Kosovichev, A. G., & Zharkova, V. V. 2001, ApJ, 550, L105
Lemen, J. R., Title, A. M., Akin, D. J., et al. 2012, Sol. Phys., 275, 17
Lin, R. P., Dennis, B. R., Hurford, G. J., et al. 2002, Sol. Phys., 210, 3
Liu, C., Deng, N., Liu, Y., et al. 2005, ApJ, 622, 722
Liu, R., & Wang, H. 2010, ApJ, 714, L41
Maričić, D., Vršnak, B., Stanger, A. L., et al. 2007, Sol. Phys., 241, 99
McKenzie, D. E., & Hudson, H. S. 1999, ApJ, 519, L93
Neupert, W. M. 1968, ApJ, 153, L59
Patterson, A. 1984, ApJ, 280, 884
Petrie, G. J. D. 2012, Sol. Phys., (arXiv:1202.4192)
Petrie, G. J. D., & Sudol, J. J. 2010, ApJ, 724, 1218
Priest, E. R., & Forbes, T. G. 2002, A&AR, 10, 313
Qiu, J., & Gary, D. E. 2003, ApJ, 599, 615
Scherrer, P. H., Bogart, R. S., Bush, R. I., et al. 1995, Sol. Phys., 162, 129
Schou, J., Scherrer, P.H., Bush, R.I., et al. 2012, Sol. Phys., 275, 229
Spirock, T. J., Yurchyshyn, V., & Wang, H. 2002, ApJ, 572, 1072
Sudol, J. J., & Harvey, J. W. 2005, ApJ, 635, 647
Sun, X., Hoeksema, J. T., Liu, Y., et al. 2012, ApJ, 748, 77
Švestka, Z. F., Fontenla, J. M., Machado, M. E., Martin, S. F., & Neidig, D. F. 1987, Sol. Phys., 108, 237
Veronig, A. M., Vršnak, B., Dennis, B. R., et al. 2002a, A&A, 392, 699
Veronig, A. M., Vršnak, B., Temmer, M., & Hanslmeier, A. 2002b, Sol. Phys., 208, 297
Wang, H. 2006, ApJ, 649, 490
Wang, H., & Liu, C. 2010, ApJ, 716, L195
Wang, H., Spirock, T. J., Qiu, J., et al. 2002, ApJ, 576, 497
Wang, S., Liu, C., Liu, R., Deng, N., Liu, Y., & Wang, H. 2012, ApJ, 745, L17
Wang, Y., & Zhang, J. 2007, ApJ, 665, 1428
Yashiro, S., Akiyama, S., Gopalswamy, N., & Howard, R.A. 2006, ApJ, 650, L143
Yashiro, S., Gopalswamy, N., Michalek, G., et al. 2004, J. Geophys. Res., 109, A07105
Zhang, J., Dere, K. P., Howard, R. A., Kundu, M. R., & White, S. M. 2001, ApJ, 559, 452

DISTRIBUTION LIST

DTIC/OCP
8725 John J. Kingman Rd, Suite 0944
Ft Belvoir, VA 22060-6218   1 cy

AFRL/RVIL
Kirtland AFB, NM 87117-5776   2 cys

Official Record Copy
AFRL/RVBXS/Edward W. Cliver   1 cy

This page is intentionally left blank.